A Robotic Cadaveric Gait Simulator With Fuzzy Logic Vertical Ground Reaction Force Control

Patrick M. Aubin, *Member, IEEE*, Eric Whittaker, and William R. Ledoux

***Abstract*—Lower limb dynamic cadaveric gait simulators are useful to investigate the biomechanics of the foot and ankle, but many systems have several common limitations, which include simplified tendon forces, nonphysiologic tibial kinematics, greatly reduced velocities, scaled body weight (BW), and, most importantly, trial-and-error vertical ground reaction force (vGRF) control. This paper presents the design, development, and validation of the robotic gait simulator (RGS), which addresses these limitations. A 6-degrees-of-freedom (6-DOF) parallel robot was utilized as part of the RGS to recreate the relative tibia to ground motion. A custom-designed nine-axis proportional-integral-derivative (PID) force-control tendon actuation system provided force to the extrinsic tendons of the cadaveric lower limb. A fuzzy logic vGRF controller was developed, which altered tendon forces in real time and iteratively adjusted the robotic trajectory in order to track a target vGRF. The RGS was able to accurately reproduce 6-DOF tibial kinematics, tendon forces, and vGRF with a cadaveric lower limb. The fuzzy logic vGRF controller was able to track the target *in vivo* vGRF with an average root-mean-square error of only 5.6% BW during a biomechanically realistic 3/4 BW, 2.7-s stance phase simulation.**

***Index Terms*—Force control, gait simulation, medical robots and systems, neural and fuzzy control, parallel robotics.**

I. Introduction

THE foot and ankle are complex in both their anatomy and function. During the stance phase of gait, the tibia has 6-degrees-of-freedom (DOF) motion, while the plantar surface of the foot interacts with the ground, creating a 3-D ground reaction force (GRF), free moment, and dynamic pressure distribution. The twelve extrinsic muscles of the lower limb continuously change force to actively provide balance, stability, and propulsion. The foot has 26 small, intricately shaped bones that form many joints with complex kinematics.

Dynamic cadaveric *in vitro* gait simulators have been employed to further our understanding of the foot and ankle's normal and pathologic function [1]–[6], investigate disease [7] and injury [8] etiology, evaluate surgical treatments [9]–[11], and explore prosthetic gait [12]. However, to accurately mimick the motion, forces, torques, and pressure distributions of the foot and ankle *in vitro* is challenging, and many systems suffer from several limitations, including 1) simplified tendon actuation, 2) nonphysiologic tibial kinematics, 3) greatly reduced velocities, 4) scaled body weight (BW), and 5) open-loop vertical GRF (vGRF) control.

Tibial kinematics often have only 3-DOF controlled to help simplify the design of complex custom-made gait simulators [1]–[6]. In contrast, a group which employed an industrial robot developed a 6-DOF gait simulator [7]. Similarly, the number of extrinsic tendons independently actuated has previously been reduced to five [7], six [1], [3], [6], seven [4], [5], or eight [2] in order to simplify mechanical design.

The simulation of the stance phase of gait with a cadaveric model at biomechanically realistic velocities has also been challenging. The fastest simulator known to the authors recently operated at 2 s impressively, which is only three to four times slower than *in vivo*, but the *in vitro* vGRF lacked the characteristic second propulsion peak seen *in vivo* [2]. Other systems with more biomechanically realistic vGRFs have performed at 3.2 [7], 10 [10], ∼12 [3], [6], 20 [1], and 60 s [4], [5].

Scaling the vGRF to less than the BW is another limitation of many gait simulators. Full BW cadaveric simulations require a strong simulation apparatus with large, expensive, high force actuators, and younger, more robust cadaveric feet. The former was given as the reason the vGRF was scaled to a peak force of only 340–590 N (i.e., equal to a BW of approximately 31.7–54.7 kg) [2] and on average 42.7 kg [7]. The latter, namely that most cadaveric specimens that are acquired are old, frail, and easily fail, was reported by several groups as the reason they performed simulations at 40% BW [1], 37.3 kg [10], and 34.8 kg [4], [5]. Other investigators have simulated 100% BW, but used lightweight donors, i.e., BWs ranging from ∼35 to ∼54 kg [3], [6].

Manuscript received June 24, 2010; revised May 4, 2011; accepted August 3, 2011. Date of publication September 29, 2011; date of current version February 9, 2012. This paper was recommended for publication by Associate Editor E. Guglielmelli and Editor J.-P. Laumond upon evaluation of the reviewers' comments. This work was supported by the VA Rehabilitation Research and Development Service under Grant A2661C, Grant A3923R, Grant A4843C, and Grant A6669R.

P. M. Aubin was with the University of Washington, Department of Electrical Engineering, Seattle, WA 98195 USA, and the Department of Veterans Affairs, RR&D Center of Excellence for Limb Loss Prevention and Prosthetic Engineering, VA Puget Sound Health Care System, Seattle, WA 98108 USA. He is now with the Department of Biomechanics, Vilnius Gediminas Technical University, Vilnius LT-01134, Lithuania (e-mail: patrickmarkaubin@gmail.com).

E. Whittaker is with the Department of Veterans Affairs, RR&D Center of Excellence for Limb Loss Prevention and Prosthetic Engineering, VA Puget Sound Health Care System, Seattle, WA 98108 USA (e-mail: whittaker.eric@gmail.com).

W. R. Ledoux is with the Department of Veterans Affairs, RR&D Center of Excellence for Limb Loss Prevention and Prosthetic Engineering, VA Puget Sound Health Care System, Seattle, WA 98108 USA, and also with the Department of Mechanical Engineering and the Department of Orthopaedics and Sports Medicine, University of Washington, Seattle, WA 98195 USA (e-mail: wrledoux@u.washington.edu).

This paper has supplementary downloadable material available at http://ieeexplore.ieee.org. provided by the author. The material includes one video MPEG-4 its frame size is 640 x 480 of duration 61 seconds. The size of the video is not specified. Minimum requirements are: Windows Media Player v12 with DirectShow-compatible MPEG-4 decoder packs installed, Real Player(win32) v14, DivX Plus for windows, QuickTime v7.6.5. Contact email wrledoux@u.washington.edu for further questions about this work.

Color versions of one or more of the figures in this paper are available online at http://ieeexplore.ieee.org.

Digital Object Identifier 10.1109/TRO.2011.2164958

Lower limb cadaveric gait simulators aim to reproduce a normative vGRF *in vitro*, yet the majority of these systems use an open-loop trial-and-error method to achieve the desired vGRF [1]–[3], [6], [10]. Open-loop trial-and-error vGRF control is an iterative process, whereby the tendon forces and/or tibial kinematics are adjusted ad hoc to achieve the desired vGRF. This method has been described by various groups as a manual iterative process [10], tuning procedure [13], exhaustive preliminary experiments [4], or repeated simulations [1]. During these simulations, the operator uses their expert knowledge of lower limb muscle and joint function to make educated trial-and-error guesses as to which muscle or kinematic input should be adjusted to achieve the desired vGRF. Compared with a trial-and-error method, closed-loop feedback control of the vGRF would likely improve the *in vitro* vGRF tracking accuracy and reduce the number of preliminary tuning simulations necessary to achieve vGRF tracking.

Given the variety of controllers that could be employed to prescribe the vGRF, a fuzzy logic control system is well suited for our application. A fuzzy logic controller can leverage the expert knowledge that we have acquired from prior gait simulations [10], [12] by embedding these heuristics into the fuzzy logic rule base [14]. Furthermore, a fuzzy logic vGRF controller can address four major challenges of the system, namely that it is 1) nonlinear, 2) ill defined, 3) underdetermined, and 4) a multiple-input and output system. As a model-free paradigm, a fuzzy rule-based controller is well suited for highly nonlinear multiple-input multiple-output systems [15]. A fuzzy logic force control system that was recently developed by Tain to investigate the load-displacement characteristics of the human spine using a robotic testing system was also recently shown to outperform hybrid control [16].

While neural networks, genetic algorithms, and other computational algorithms could not utilize our prior expert knowledge as directly as fuzzy logic control, they could address the four major challenges that are listed earlier. However, they are unsuitable for our specific application for other reasons. Unlike a computational model, which can be used thousands of times repeatedly, a cadaveric model degrades rapidly with use. Typically, a cadaveric foot can be used for 2–5 days and at most for approximately 100 simulations. Old frail feet degrade even quicker and sometimes last no longer than a few simulations. Thus, any control system, such as an artificial neural network, that requires repeated simulations or the generation of a large dataset for training is not well suited for a cadaveric model. To perform a large number of cadaveric simulations would require both an exorbitant amount of time and specimens.

Thus, in review of these considerations, the aim of this study was to develop a robotic gait simulator (RGS) with closed-loop fuzzy logic vGRF control, which has the ability to 1) actuate nine extrinsic tendons, 2) prescribe 6-DOF physiologic tibial kinematics, 3) operate at biomechanically more realistic speeds, and 4) accurately simulate larger vGRFs.

II. Methods

A. Living Subject Gait Data Collection

Kinematic and kinetic gait data were collected from ten living subjects performing four or five repeated gait trials in our motion analysis laboratory. A 12-camera motion analysis system (Vicon, Lake Forest, CA) recorded the rigid body motion of the tibia (TIB) with respect to the laboratory ground coordinate system (GND). The tibial motion was described with a time-dependent 4×4 homogeneous transformation matrix $T_{\mathrm{GNDTIB}}(n)$. A force plate (Bertec Corporation, Columbus, OH) sampling at 600 or 1500 Hz recorded the GRF. *In vivo* musculotendinous forces were estimated from values that are reported in the literature for the muscles' physiological cross-sectional area (in square centimeters) [17], maximum specific isometric tension (in newtons per square centimeter) [18], activation level (in percent) [19], and electromechanical delay [20]. The Achilles (Ach) tendon force was taken from [21], where it was measured directly.

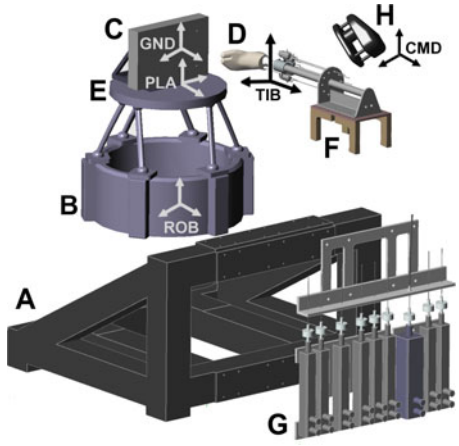

Fig. 1. Exploded view of the RGS with (A) surrounding frame; (B) motor attached to R2000 base; (C) mobile force plate; (D) cadaveric foot; (E) mobile top plate; (F) tibia mounting device; (G) tendon actuation system; and (H) six-camera motion analysis system with only one camera shown. The coordinate systems shown are the ground (GND), plate (PLA), robot base (ROB), tibia (TIB), and motion analysis system (CMD).

B. Robotic Gait Simulator

The RGS consists of an R2000 6-DOF parallel robot (Mikrolar Inc., Hampton, NH), nine brushless DC linear tendon force actuators (Exlar Corporation, Chanhassen, MN) in series with nine load cells (Transducer Techniques Inc., Temecula, CA), a force plate (Kistler Instrument Corporation, Amherst, NY), a real-time peripheral component interconnect extensions for instrumentation (PXI)-embedded controller (National Instruments Corporation, Austin, TX), and a PC user interface (see Fig. 1). The RGS uses inverse motion between the cadaveric tibia and the ground. To simulate gait, the tibia was held fixed in place, while the R2000 moved the force plate to recreate the relative tibia to ground motion. Tendon force was controlled by a real-time nine-axis PID force controller running on the PXI. The robot motion and GRF data acquisition, tendon force, and six-camera motion analysis system (Vicon, Lake Forest, CA) were synchronized to a 5-V trigger at heel strike.

C. Fuzzy Logic Vertical Ground Reaction Force Control

A fuzzy logic controller has three steps: fuzzification, inference, and defuzzification. Fuzzification is the conversion of a numerical value of the input variables into a corresponding

linguistic value by the association of a membership degree via a membership function. Inference uses a fuzzy implication method, such as minimum or Mamdani [22], and a fuzzy rule base to determine a fuzzy output set based on the input variables. Defuzzification is the process to determine a crisp output value from a fuzzy output set using a method, such as center of gravity (COG) [23]. The fuzzy logic control is suitable for ill-defined systems, where human experience is available for control-rule synthesis [14]

The fuzzy logic vGRF controller was comprised of three distinct multiple-input single-output fuzzy logic controller blocks, namely 1) an Ach tendon force controller, 2) a tibialis anterior (TA) tendon force controller, and 3) a force-plate-position controller. Previous trial-and-error simulation adjustments to TA's force and to the force plate's position were shown to affect the first peak of the vGRF, while adjustments to the Ach tendon force affected the second peak of the vGRF [10]. The vGRF during the entire stance phase of gait was controlled by the adjustment of the force plate's position, TA's force, and Ach's force at various times in the stance phase. Thus, the percent stance phase (*stance*) was chosen as an input variable.

The membership functions for the percent stance phase variable (*stance*) were based on physiological events that occur during the stance phase of gait. Heel strike is the moment the heel strikes the ground and the vGRF quickly increases. From heel strike to foot flat, the center of pressure is posterior to the ankle joint, creating a negative ankle-joint torque (plantar flexion torque) [19]. During this time, TA is active, slowing the plantar flexion of the ankle and advancing the tibia forward in the sagittal plane. Foot flat occurs at 16.6% of the stance phase when the forefoot touches the ground [19]. After foot flat, TA's force decreases, while the Ach tendon force increases, causing the center of pressure to move anteriorly until it is underneath the metatarsal heads at 43.5% of the stance phase [19]. As the center of pressure advances anteriorly, i.e., away from the ankle joint, the ankle-joint torque increases (dorsiflexion torque). Shortly after, at 50% of the stance, heel rise occurs, while the Ach tendon force and ankle-joint torque continue to increase. With the heel raised, the center of pressure remains underneath the metatarsophalangeal joints, which act as a rocker for the foot until the contralateral limb strikes the ground at 83% of the stance phase [19]. Heel strike of the contralateral limb quickly unloads the ipsilateral limb, the center of pressure moves anterior of the metatarsophalangeal joints, and TA becomes active, preparing the limb for the swing phase of gait. The stance phase of gait ends with toe off. Based on these events, the *stance* variable, which had a range of 0–100%, was partitioned into the following four fuzzy sets: *heel strike* (0–3.3%), *load response* (3.3–16.6%), *midstance* (16.6–43.5%), and *late stance* (43.5–100%) (see Fig. 2). The membership functions for each fuzzy set were piecewise linear.

The Ach tendon fuzzy logic controller had the following three inputs: percent stance phase, i.e., *stance*; the vGRF error, i.e., $\mathrm{vGRF}_{\mathrm{error}}$; and the integral of the vGRF error, i.e, $\Sigma\mathrm{vGRF}_{\mathrm{error}}$. The $\mathrm{vGRF}_{\mathrm{error}}$ and $\Sigma\mathrm{vGRF}_{\mathrm{error}}$ inputs were partitioned into three fuzzy sets: negative (*N*), zero (*Z*), and positive (*P*) (see Fig. 3). The range of the input variables $\mathrm{vGRF}_{\mathrm{error}}$ and

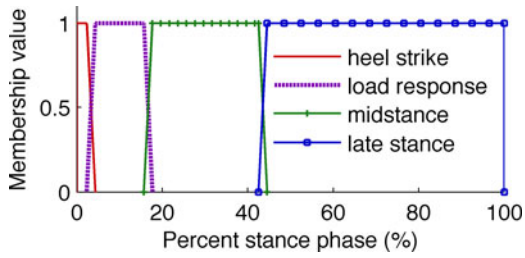

Fig. 2. Membership functions for *heel strike*, *load response*, *midstance*, and *late stance* fuzzy sets.

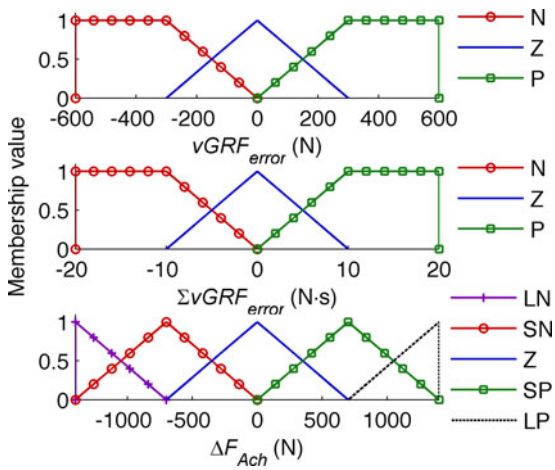

Fig. 3. Ach tendon fuzzy logic controller's membership functions for the two inputs $\mathrm{vGRF}_{\mathrm{error}}$ and $\Sigma\mathrm{vGRF}_{\mathrm{error}}$, and the output ΔF_{Ach}. The fuzzy sets are large negative LN, small negative SN, negative N, zero Z, positive P, small positive SP, and large positive LP.

$\Sigma\mathrm{vGRF}_{\mathrm{error}}$ was ± 600 N and ± 20 N·s, respectively, for the Ach fuzzy logic controller (see Fig. 3). The Ach tendon fuzzy logic controller's membership functions were piecewise linear.

The output of the Ach tendon fuzzy logic controller was a change in the Ach tendon force ΔF_{Ach} with a range of ± 1400 N. The output variable ΔF_{Ach} was partitioned into the following five fuzzy sets: large negative LN, small negative SN, zero (*Z*), small positive SP, and large positive LP (see Fig. 3). The membership functions were piecewise linear.

The rule base for the ΔF_{Ach} fuzzy logic controller (see Table I) was designed so that when *stance* has membership in *late stance*, the vGRF is controlled via adjustments to the target Ach tendon force. When *stance* has membership in the *heel strike*, *load response*, or *midstance* fuzzy sets, the rule base stated that ΔF_{Ach} will be zero. For each activated fuzzy rule, a minimum inference method was performed, followed by a maximum composition and a COG defuzzification to determine a crisp ΔF_{Ach} control output.

The TA tendon fuzzy logic controller had the following three inputs: percent stance phase (*stance*) (see Fig. 2), the vGRF error, i.e., $\mathrm{vGRF}_{\mathrm{error}}$, and the integral of the vGRF error, i.e., $\Sigma\mathrm{vGRF}_{\mathrm{error}}$. The $\mathrm{vGRF}_{\mathrm{error}}$ and $\Sigma\mathrm{vGRF}_{\mathrm{error}}$ inputs were partitioned into the following three fuzzy sets: *N*, *Z*, and *P* (see Fig. 4). The range of the input variables $\mathrm{vGRF}_{\mathrm{error}}$ and $\Sigma\mathrm{vGRF}_{\mathrm{error}}$ were ± 600 N and ± 40 N·s, respectively, (see Fig. 4). The TA

TABLE I
RULE BASE FOR THE CONTROL OUTPUT ΔF_{Ach} WHEN *stance* HAS MEMBERSHIP IN *late stance*

	$\sum vGRF_{error}$		
$vGRF_{error}$	N	Z	P
N	$LN\Delta F_{Ach}$	$SN\Delta F_{Ach}$	$Z\Delta F_{Ach}$
Z	$SN\Delta F_{Ach}$	$Z\Delta F_{Ach}$	$SP\Delta F_{Ach}$
P	$Z\Delta F_{Ach}$	$SP\Delta F_{Ach}$	$LP\Delta F_{Ach}$

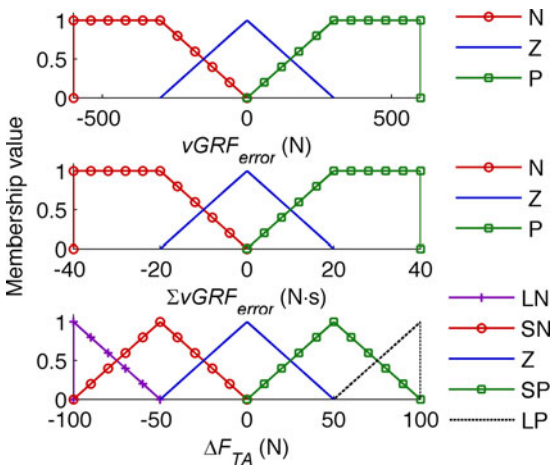

Fig. 4. TA fuzzy logic controller's membership functions for input variables $\mathrm{vGRF_{error}}$ and $\Sigma\mathrm{vGRF_{error}}$ and output variable ΔF_{TA}. The fuzzy sets are large negative LN, small negative SN, negative *N*, zero *Z*, positive *P*, small positive SP, and large positive LP.

TABLE II
RULE BASE FOR THE CONTROL OUTPUT ΔF_{TA} WHEN *stance* HAS MEMBERSHIP IN THE *heel strike* OR *load response*

	$\sum vGRF_{error}$		
$vGRF_{error}$	N	Z	P
N	$LN\Delta F_{TA}$	$SN\Delta F_{TA}$	$Z\Delta F_{TA}$
Z	$SN\Delta F_{TA}$	$Z\Delta F_{TA}$	$SP\Delta F_{TA}$
P	$Z\Delta F_{TA}$	$SP\Delta F_{TA}$	$LP\Delta F_{TA}$

tendon fuzzy logic controller's membership functions were piecewise linear.

The output of the TA controller was a change in the TA tendon force ΔF_{TA} with a range of ± 100 N. The output variable ΔF_{TA} was partitioned into the following five fuzzy sets: LN, SN, *Z*, SP, and LP (see Fig. 4). The membership functions were piecewise linear.

The rule base for the ΔF_{TA} fuzzy logic controller was designed so that when *stance* has membership in the *heel strike* or *load response* sets, the vGRF is controlled via adjustments to the target TA tendon force (see Table II). When *stance* has membership in the *midstance* or *late stance* fuzzy sets, the rule base stated that ΔF_{TA} will be zero.

For each activated fuzzy rule, a minimum inference method was performed, followed by a maximum composition and a COG defuzzification to determine a crisp ΔF_{TA} control output.

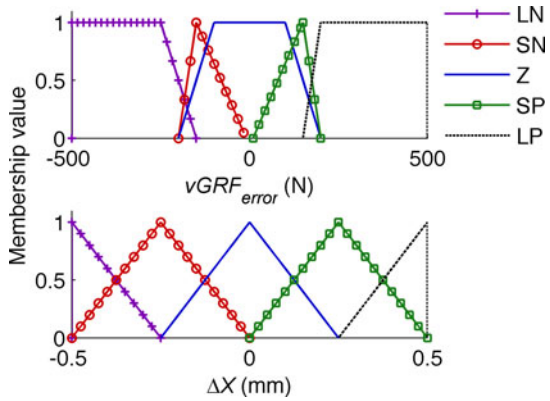

Fig. 5. Force-plate-position fuzzy logic controller's membership functions input $\mathrm{vGRF_{error}}$ and output Δx. The fuzzy sets are large negative LN, small negative SN, zero *Z*, small positive SP, and large positive LP.

TABLE III
RULE BASE FOR THE CONTROL OUTPUT ΔX

	stance			
$vGRF_{error}$	*heel strike*	*load response*	*midstance*	*late*
LN	$Z\Delta x$	$LN\Delta x$	$LN\Delta x$	$Z\Delta x$
SN	$Z\Delta x$	$SN\ \Delta x$	$SN\Delta x$	$Z\Delta x$
Z	$Z\Delta x$	$Z\Delta x$	$Z\Delta x$	$Z\Delta x$
SP	$Z\Delta x$	$SP\Delta x$	$SP\ \Delta x$	$Z\Delta x$
LP	$Z\Delta x$	$LP\Delta x$	$LP\ \Delta x$	$Z\Delta x$

The change in force–plate-position fuzzy logic controller had one input, i.e., $\mathrm{vGRF_{error}}$, with a range of ± 500 N and one output Δx, with a range of ± 0.5 mm (see Fig. 5). The $\mathrm{vGRF_{error}}$ input was partitioned into the following five fuzzy sets: LN, SN, *Z*, SP, and LP. The Δx output was partitioned into the following five sets: LN, SN, *Z*, SP, and LP (see Fig. 5).

The rule base for the Δx fuzzy logic vGRF controller was designed so that when *stance* has membership in the *load response* or *midstance* sets, the vGRF is controlled via adjustments to Δx (see Table III). When *stance* has membership in the *heel strike* or *late stance* fuzzy sets, the rule base stated that Δx will be zero. For each activated fuzzy rule, a minimum inference method was performed, followed by a maximum composition and a COG defuzzification to determine a crisp Δx control output.

The membership functions for the $\mathrm{vGRF_{error}}$ were designed to achieve a nonlinear Δx response for a given $\mathrm{vGRF_{error}}$. Because of the nonlinear properties of the plantar fat, the stiffness increases with increasing strain [24]. The nonlinear Δx response accommodates the cadaveric foot's nonlinear stiffness by assumption that if the $\mathrm{vGRF_{error}}$ is large, the system is operating in an area of low stiffness and larger Δx responses are warranted. A small $\mathrm{vGRF_{error}}$ means the system is operating in an area of high stiffness and the Δx output should be smaller.

In contrast with the ΔF_{Ach} and ΔF_{TA} controllers, the Δx fuzzy logic vGRF controller was an iterative rather than a real-time controller. The output from the fuzzy logic controller for the simulation $j-1$ was written as $\Delta x(n)_{j-1}$ and used to alter the R2000's *j*th simulation trajectory. The R2000's trajectory

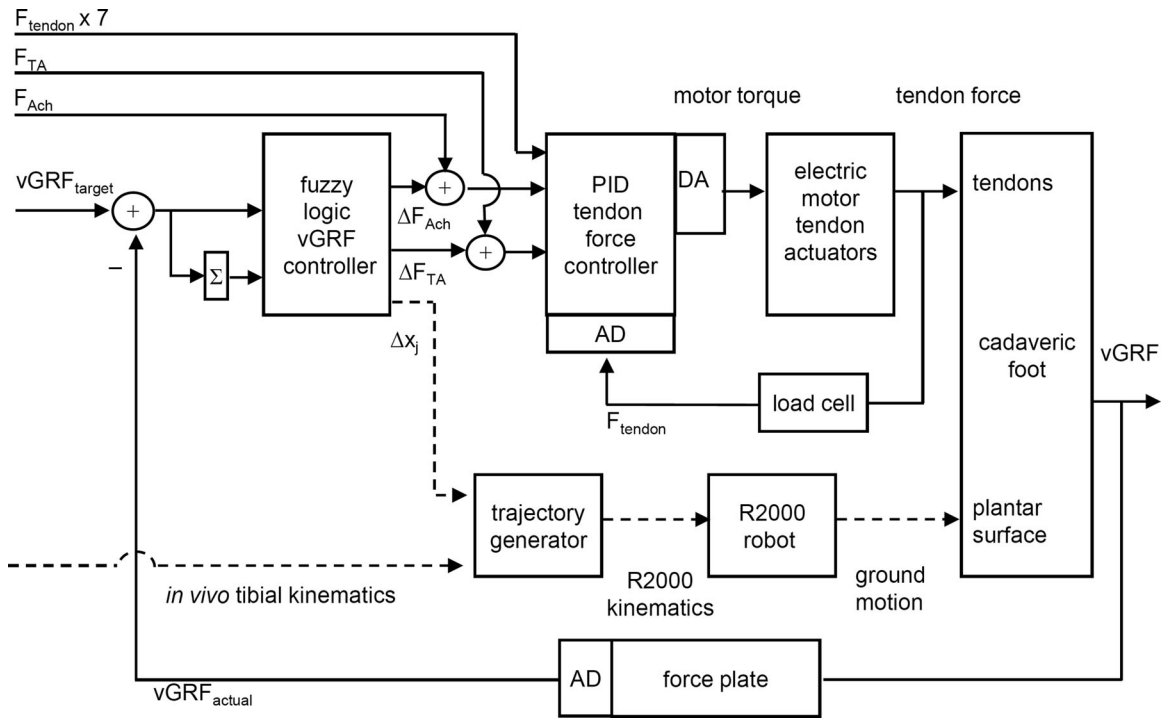

Fig. 6. Block diagram of the RGS fuzzy logic vGRF controller. The controller's output ΔF_{Ach} and ΔF_{TA} were added to the *in vivo* Ach and TA tendon force estimate, respectively, and sent to the PID tendon force controller as the target tendon force. The controller's output $\Delta x(n)_j$ is shown as a dotted line because it was updated iteratively rather than in real time.

for the *j*th simulation was described by $T_{\mathrm{ROB\,PLA}}(n)_j$, i.e., the 4×4 homogeneous transformation matrix representation of the pose of the R2000's plate (PLA) coordinate system with respect to the robot coordinate system (ROB). The time-dependent transformation matrix for the *j*th simulation $T_{\mathrm{ROB\,PLA}}(n)_j$ was written as

$$T_{\mathrm{ROB\,PLA}}(n)_j = \begin{bmatrix} R_{\mathrm{ROB\,PLA}}(n)_j & q_{\mathrm{ROB\,PLA}}(n)_j \\ 0 & 1 \end{bmatrix} \quad (1)$$

where $R_{\mathrm{ROB\,PLA}}(n)_j$ and $q_{\mathrm{ROB\,PLA}}(n)_j$ specify the rotation matrix and translation vector of the PLA with respect to the ROB, respectively. After each simulation with learning was complete, the iteration domain R2000 trajectory update control law (2) was used to create a new R2000 trajectory for the next simulation. The control law maintained the same angular relationship between the GND and the TIB but translated the GND origin by an amount $\Delta x(n)_{j-1}$ along its *x*-axis, i.e., the axis normal to the force plate surface.

$$T_{\mathrm{ROB\,PLA}}(n)_j = \begin{matrix} R_{\mathrm{ROB\,PLA}}(n)_1 & q_{\mathrm{ROB\,PLA}}(n)_{j-1} + R_{\mathrm{ROB\,PLA}}(n)_1 \cdot \Delta x(n)_{j-1} \\ 0 & 1 \end{matrix} \quad (2)$$

The fuzzy logic vGRF controller was developed using Labview's fuzzy logic toolbox and deployed on a PXI-embedded real-time controller. The ΔF_{Ach} and ΔF_{TA} output of the fuzzy logic controller was added to the *in vivo* estimate of Ach and TA tendon forces, respectively, and sent to the PID tendon-force controller as the target tendon forces (see Fig. 6). The $\Delta x(n)$ output from the fuzzy logic vGRF controller was filtered with a second-order 5-Hz Butterworth low-pass filter and used to update the R2000 trajectory iteratively between gait simulations (see Fig. 6).

Preliminary simulations using a modified endoskeletal single-axis prosthetic foot (Ohio Willow Wood, Mt. Sterling, OH) were performed, while manually adjustment of the range of the fuzzy set until the satisfactory vGRF tracking was attained.

D. Trajectory Optimization

Before simulations could be performed, the cadaveric specimen had to be registered to the R2000, and the appropriate robotic trajectory had to be determined. Tibial registration and trajectory optimization was a process that sought to determine the R2000 trajectory. This produced the desired TIB with respect to GND motion, while keeping the PLA trajectory $T_{\mathrm{ROB\,PLA}}$ within the working volume of the R2000 and minimizing the peak R2000 motor velocity. To perform the registration and optimization, a tibial coordinate system was constructed from the four markers attached to the tibia. The coordinate system was consistent with the ISB standard, with the *x*-axis that points anteriorly, *y*-axis that points superiorly, and *z*-axis that points medially for a left foot and laterally for a right foot. A six-camera motion analysis system was used to determine the pose of TIB with respect to CMD, i.e., the 4×4 homogeneous transformation matrix $T_{\mathrm{CMD\,TIB}}$:

$$T_{\mathrm{CMD\,TIB}} = \begin{bmatrix} R_y(\theta_y)R_x(\theta_x)R_z(\theta_z) & q_{\mathrm{CMD\,TIB}} \\ 0 & 1 \end{bmatrix}. \quad (3)$$

The pose of the CMD with respect to the ROB frame $T_{\mathrm{ROB\,CMD}}$ was explicitly known based on the calibration of the Vicon camera system. The time-independent pose of the PLA frame with respect to the GND frame $T_{\mathrm{GND\,PLA}}$ was explicitly known based on the mounting of the force plate and the selection of the location of GND on the surface of the force plate. Given these three transformations and the recorded *in vivo* tibia kinematics $T_{\mathrm{TIB\,GND}}(n)$, the time-dependent R2000 trajectory $T_{\mathrm{ROB\,PLA}}(n)$ was calculated as

$$T_{\mathrm{ROB\,PLA}}(n) = T_{\mathrm{ROB\,CMD}} \cdot T_{\mathrm{CMD\,TIB}} \cdot T_{\mathrm{TIB\,GND}}(n) \cdot T_{\mathrm{GND\,PLA}}. \quad (4)$$

The R2000's inverse kinematic map $g^{-1}(\cdot)$ was then used to calculate the R2000 motor displacements per time step, a value proportional to the motor velocity, in units of motor encoder counts, $\Delta\vartheta(\mathrm{counts}) \in \boldsymbol{R}^6$, for the given R2000 trajectory $T_{\mathrm{ROB\,PLA}}(n)$:

$$\Delta\vartheta(n) = g^{-1}(T_{\mathrm{ROB\,PLA}}(n)) - g^{-1}(T_{\mathrm{ROB\,PLA}}(n-1)). \quad (5)$$

The maximum motor displacement per time step $\Delta\vartheta_{\max}(\mathrm{counts}) \in \boldsymbol{R}^1$, for a given $T_{\mathrm{ROB\,PLA}}(n)$ trajectory, was determined by

$$\Delta\vartheta_{\max}(\mathrm{counts}) = ||\max(\Delta\vartheta(n))||_\infty \quad (6)$$

i.e., the infinity norm of the maximum value of $\Delta\vartheta(n)$ over all n. Combining (4)–(6) gives the full expression for $\Delta\vartheta_{\max}$:

$$\begin{aligned}\Delta\vartheta_{\max} = ||\max(&g^{-1}\left(T_{\mathrm{ROB\,CMD}} \cdot T_{\mathrm{CMD\,TIB}} \cdot T_{\mathrm{TIB\,GND}}(n)\right.\\ &\left.\cdot T_{\mathrm{GND\,PLA}}\right) - g^{-1}\left(T_{\mathrm{ROB\,CMD}} \cdot T_{\mathrm{CMD\,TIB}}\right.\\ &\left.\cdot T_{\mathrm{TIB\,GND}}(n-1) \cdot T_{\mathrm{GND\,PLA}}\right))||_\infty. \quad (7)\end{aligned}$$

The maximum motor displacement per time interval $\Delta\vartheta_{\max}$ was minimized by positioning the tibia into an optimal $T_{\mathrm{CMD\,TIB}}$ pose. Not all six DOFs in $T_{\mathrm{CMD\,TIB}}$ and $T_{\mathrm{GND\,PLA}}$ could be varied in order to minimize $\Delta\vartheta_{\max}$ because the RGS tibia mounting system only allowed for easy adjustments to the internal–external rotation of the tibia θ_x and the superior–inferior translation of the tibia with respect to CMD $q_{\mathrm{CMD\,TIB}_z}$. Similarly, the GND frame was required to be on the surface of the force plate and parallel to the force plate but could have a varied medial–lateral position $q_{\mathrm{GND\,PLA}_x}$ or anterior–posterior position $q_{\mathrm{GND\,PLA}_z}$. After the cadaveric foot was secured into the tibia pot and mounted onto the RGS, four variables, i.e., θ_x, $q_{\mathrm{CMD\,TIB}_x}$, $q_{\mathrm{GND\,PLA}_x}$, and $q_{\mathrm{GND\,PLA}_z}$ were altered by repositioning the tibia or changing the GND position in order to minimize the maximum motor displacement $\Delta\vartheta_{\max}$.

An exhaustive search optimization routine was employed to find values of θ_x, $q_{\mathrm{CMD\,TIB}_x}$, $q_{\mathrm{GND\,PLA}_x}$, and $q_{\mathrm{GND\,PLA}_z}$, which minimized $\Delta\vartheta_{\max}$ for a given $T_{\mathrm{TIB\,GND}}(n)$ trajectory:

$$\begin{aligned}&[\theta_x\ q_{\mathrm{CMD\,TIB}_x}\ q_{\mathrm{GND\,PLA}_x}\ q_{\mathrm{GND\,PLA}_z}]_{\mathrm{optimal}}\\ &\qquad = \underset{\theta_x\ q_{\mathrm{CMD\,TIB}_x} q_{\mathrm{GND\,PLA}_x}\ q_{\mathrm{GND\,PLA}_z}}{\arg\min} (\Delta\vartheta_{\max}). \quad (8)\end{aligned}$$

A finite search grid over which the minimization was performed was created with a step size of 2°, 5 mm, 5 mm, and 10 mm for θ_x, $q_{\mathrm{CMD\,TIB}_x}$, $q_{\mathrm{GND\,PLA}_x}$, and $q_{\mathrm{GND\,PLA}_z}$, respectively.

After the optimization was complete, the cadaveric foot was repositioned to be roughly equal to the optimal pose using the tibial mounting device. The exact pose of the tibia $T_{\mathrm{CMD\,TIB}}$ was determined once again with the six-camera motion analysis system and repositioning was repeated as necessary. The final value of $T_{\mathrm{CMD\,TIB}}$ was used in (4) to determine the optimized R2000 trajectory used for subsequent simulations.

E. Cadaveric Simulations

Six cadaveric lower limb specimens, i.e., five male and one female, with a mean age of 75.8 years (range 69–85 years) and a mean BW of 62.2 kg (range 59–68.1 kg) were acquired for this Institutional Review Board (IRB)-approved study. Approximately 10 cm of the extensor hallucis longus (EHL), extensor digitorum longus (EDL), TA, tibialis posterior (TP), flexor hallucis longus (FHL), flexor digitorum longus (FDL), peroneus brevis (PB), and peroneus longus (PL) tendons were dissected and attached to aluminum or plastic tendon clamps. A specially designed liquid-nitrogen freeze clamp was used on the Ach tendon for additional holding strength. A 1.27-cm diameter drill bit was used to hollow out the tibial intramedullary canal. An aluminum dowel was inserted into the canal and attached to a 4-cm diameter metal cylinder, which surrounded the proximal tibia. A 5-cm screw was drilled through the mounting device, tibia, and fibula, securing them in place, and the cylinder was filled with polymethylmethacrylate. The cadaveric was then mounted onto the RGS in the optimum pose as described earlier.

During preliminary RGS trials, a superior–inferior offset to the R2000 trajectory and the Ach tendon force gain G were adjusted iteratively to slowly increase the first and second peaks of the vGRF from zero to approximately 75% BW. Once the two vGRF peaks were roughly equal to their target peak forces, the fuzzy logic vGRF controller was enabled and a quartet of trials, three "learning" trials and one "final" trial, was performed with a recovery time of approximately 45 s between each learning trial. The four trials had the added benefit of allowing the foot tissues to precondition and to insure a more constant force deformation response. During the recovery time, the iterative fuzzy logic vGRF controller determined $\Delta x(n)_{j+1}$ for the next trial so that the *in vitro* vGRF would track the target *in vivo* vGRF. For each foot, three simulation quartets were collected.

F. Statistical Methods

Statistical analysis was performed to characterize differences between the *in vivo* and *in vitro* vGRF and TIB to GND angles. For each *in vivo* and *in vitro* trial, the following vGRF summary measures were calculated: first peak (N/BW), first peak time (%), second peak (N/BW), second peak time (%), minimum between peaks (N/BW), minimum time (%), and vGRF integral (N·s/BW). The mean vGRF and SDs for each sample point were also computed. Differences in the mean vGRF and summary measures were assessed using linear mixed effects regression with the mean vGRF or summary measure as the dependent variable, foot type as the independent variable, and foot as a random effect to account for multiple trials for each foot.

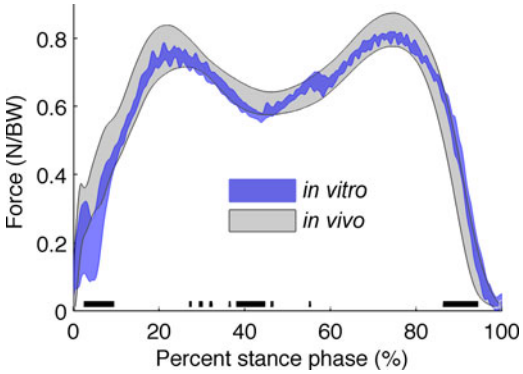

Fig. 7. Mean ±1 SD *in vitro* vGRF for all six feet with three trials per foot (blue) compared with the target mean ± 1 SD *in vivo* vGRF (gray). The black sections at the bottom indicate which samples had significant differences in the mean vGRF between the *in vivo* and *in vitro* feet.

For each *in vivo* and *in vitro* trial, mean tibia angles and SDs for each sample point were computed. Because the *in vivo* and *in vitro* trials had different sampling rates, two-sample t-tests comparing upsampled mean *in vivo* angles with the mean *in vitro* angles were carried out. All analyses were performed with R 2.9.1 [25].

III. Results

For each foot, the optimal values of $T_{\mathrm{CMD\,TIB}}$ and $T_{\mathrm{PLA\,GND}}$ were determined such that the required $T_{\mathrm{ROB\,PLA}}$ trajectory was within R2000's working volume, and the R2000's motor velocities were minimized. Of the 720 trajectories analyzed, the number of trajectories within the working volume of the R2000 ranged from 38 to 495. When comparing the optimal values of $T_{\mathrm{CMD\,TIB}}$ and $T_{\mathrm{PLA\,GND}}$ versus their worst possible values, the reduction in the maximum motor velocity ranged from 7.42% to 64.40%.

The fuzzy logic vGRF controller demonstrated its ability to accurately control the vGRF; the mean *in vitro* vGRF was within ±1 SD of the mean *in vivo* data for almost the entire stance phase (see Fig. 7). The average RMS error between the target *in vivo* and actual *in vitro* vGRF was 5.6% BW across all 18 final trials. No statistically significant differences were found between the magnitude and timing of the *in vitro* and *in vivo* vGRF first peak ($p = 0.4$ and 0.6, respectively) or second peak ($p = 0.3$ and 0.8, respectively). The mean *in vitro* vGRF minimum was 5.9% below that of *in vivo* ($p = 0.0050$); however, no difference was found in its timing ($p = 0.067$), which occurred 4.9% earlier. The integral of the *in vitro* vGRF was only 2.0% different from that of *in vivo* ($p = 0.02$). See Table IV.

The vGRF fuzzy logic controller was precise. The within specimen across trial *in vitro* vGRF variability was less than the within subject *in vivo* vGRF variability (see Fig. 8). The anterior–posterior GRF and medial–lateral GRF, although not controlled, still roughly matched that of *in vivo* (see Fig. 9).

The RGS was able to replicate the *in vivo* kinematics of the TIB with respect to GND. The sagittal-, frontal-, and transverse-plane fixed angles of the TIB with respect to the GND were almost entirely within ±1 SD of those found *in vivo* for all feet (see Fig. 10). The two-sample t-tests showed no significant difference between the target *in vivo* and actual *in vitro* tibial angles.

The RMS tracking error for the EHL, EDL, TP, FHL, FDL, PB, and PL tendons ranged from 2.6 N for FDL to 5.6 N for TP with a mean value of 3.9 N across all 18 final trials (see Fig. 11 and Table V). The mean peak Ach and TA tendon forces

TABLE IV
In vivo AND *in vitro* MEAN ±1 SD vGRF SUMMARY MEASURES

summary measure	***in vitro* ± *SD*** (n=6)	***in vivo* ± *SD*** (n=10)	% Δ	p-value
first peak (N/BW)	0.776 ± 0.023	0.789 ± 0.053	1.7	0.400
first peak time (%)	23.4 ± 1.800	24.2 ± 4.100	3.3	0.600
minimum (N/BW)	0.563 ± 0.013	0.598 ± 0.035	5.9	0.005
minimum time (%)	44.4 ± 0.900	46.7 ± 4.300	4.9	0.067
second peak (N/BW)	0.819 ± 0.006	0.834 ± 0.045	1.8	0.300
second peak time (%)	74.7 ± 2.000	74.3 ± 2.600	0.4	0.800
vGRF integral (N·s/BW)	1.602 ± 0.017	1.635 ± 0.043	2.0	0.020

Differences (% Δ) were estimated from a mixed effects model of vGRF summary measure on the foot type with random effect for foot. Given "*p*-value" is for differences in the mean summary measure by the foot type *(in vivo* versus *in vitro*).

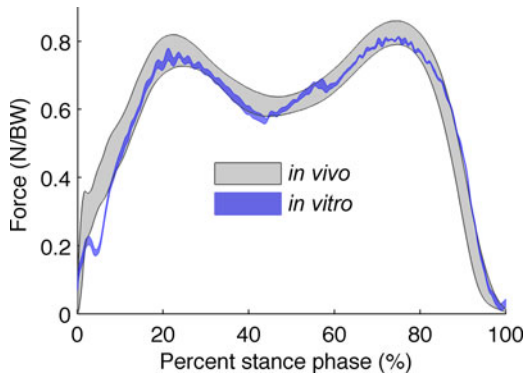

Fig. 8. Mean ±1 within subject SD for both *in vitro* (blue) and *in vivo* (gray) vGRF. The plot demonstrates the precision of the vGRF controller with the *in vitro* vGRF variability associated with differences within the specimen across trials being less than the within subject *in vivo* variability.

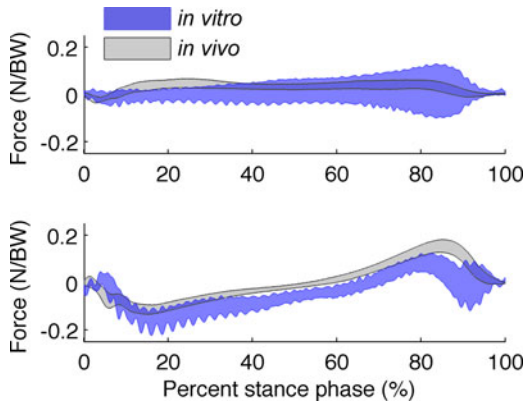

Fig. 9. Mean ±1 SD *in vitro* (blue) medial–lateral (top) and anterior–posterior (bottom) GRF compared with the target *in vivo* GRF (gray).

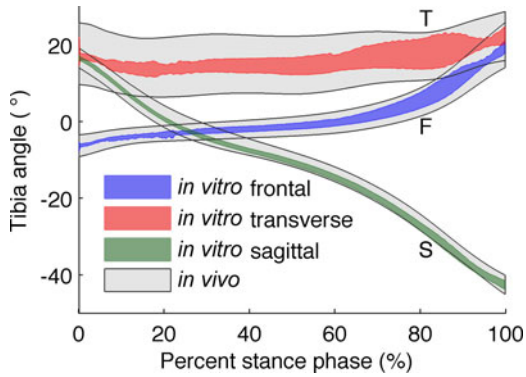

Fig. 10. Mean *in vivo* ±1 SD tibia with respect to ground fixed angles (gray) compared with mean *in vitro* ±1 SD tibia angles for the frontal (blue), transverse (red), and sagittal (green) planes for all six feet with three trials per foot. F = frontal plane, T = transverse plane, S = sagittal plane.

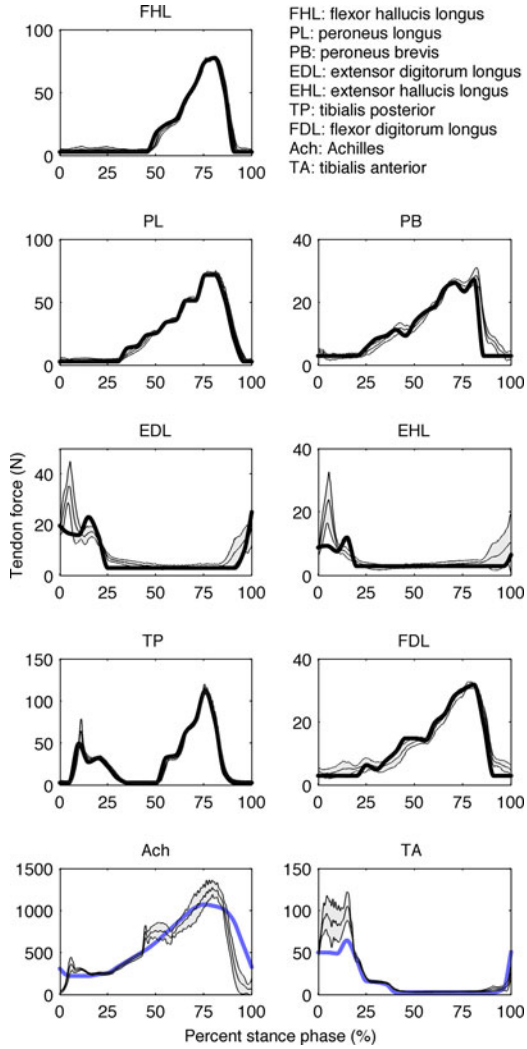

Fig. 11. Estimated *in vivo* tendon force (black) compared with mean ±1SD *in vitro* tendon force (gray). The estimated *in vivo* tendon force for Ach and TA are shown in blue because they are not the target forces; rather, the target tendon force was specified by the fuzzy logic vGRF controller.

TABLE V
In vitro TENDON FORCE TRACKING PERFORMANCE THAT IS REPORTED AS THE MEAN ROOT-MEAN SQUARE ERROR

Tendon[1]	Mean RMS error (N)	Mean RMS error as percent of peak target force (%)
EHL	3.6	30.6
EDL	5.0	19.9
TP	5.6	5.0
FHL	3.8	5.0
FDL	2.6	8.0
PB	3.2	11.8
PL	3.3	4.6

[1]Tendon are abbreviated as follows: extensor hallucis longus (EHL), extensor digitorum longus (EDL), tibialis posterior (TP), flexor hallucis longus (FHL), flexor digitorum longus (FDL), peroneus brevis (PB), and peroneus longus (PL).

were 1273.0 N at 79.4% stance and 105.1 N at 15.2% stance, respectively. The RMS tracking errors for the Ach and TA tendon forces were not calculated because their estimated *in vivo* tendon force were not the target forces, rather the target tendon force was specified in real time by the fuzzy logic vGRF controller.

IV. DISCUSSION

The recreation of high-fidelity gait kinematics and kinetics *in vitro* is a challenging complex task. During the stance phase of gait, the tibia moves with 6-DOFs, the extrinsic tendons of the lower limb have time-varying force profiles, and the GRF is time-varying with peak forces that reach above BW. Despite these challenges, several groups have developed dynamic *in vitro* gait simulators to study the biomechanics of the foot and ankle [1]–[13]. These custom-built systems have many limitations, including simplifying tibial kinematics [1]–[6]; reducing the number of independently control tendons [1]–[7]; a temporally scaled stance phase of 2 s [2], 3.2 s [7], 10 s [10], ∼12 s [3], [6], 20 s [1], and 60 s [4], [5]; a scaled vGRF of 31–55 kg, [2]–[7], [10], or 40% BW [1]; and a trial-and-error vGRF control methodology [1]–[3], [6], [10]. In this study, we overcame these limitations by leveraging an industrial robot, a nine-axis force control tendon actuation system, and advanced feedback control methods to prescribe a high-fidelity vGRF (see Table VI).

By the employment of a 6-DOF parallel robot, the tibial kinematics were tightly prescribed in six DOFs. The accuracy of the R2000 robot, which is approximately 50 μm under static loading conditions, exceeds the accuracy of the motion analysis system that is used to measure the tibial kinematics. The small variability and inaccuracy in the *in vitro* tibia kinematics compared with the target *in vivo* kinematics (see Fig. 10) are likely the result of limitations within the Vicon motion analysis system including marker placement, occlusions, and collisions but not the robot kinematics.

TABLE VI
SUMMARY OF DYNAMIC CADAVERIC GAIT SIMULATORS COMPARED WITH THE RGS. FOLLOWING ABBREVIATIONS ARE USED TO DESCRIBE THE TIBIAL KINEMATICS: SUPERIOR/INFERIOR TRANSLATION (S/I), ANTERIOR/POSTERIOR TRANSLATION (A/P), MEDIAL/LATERAL TRANSLATION (M/L), SAGITTAL PLANE ROTATION (SAG.), FRONTAL PLANE ROTATION (FRONT.), AND TRANSVERSE PLANE ROTATION (TRANS.)

System	vGRF control	vGRF scale (%)	speed (s)	number of independently actuated tendons	tibial kinematics		
					fixed	prescribed	un-constrained
Pennsylvania State Univ. [3,6,8]	open loop	100	12	6	M/L, front., trans.[1]	S/I, A/P sag.	none
Univ. of Salford & Iowa State Univ. [2, 9]	open loop	50	2	8	M/L	S/I, A/P	sag., front., trans.
Medical School of Hannover, Germany [4,5]	force control	50	60	7	A/P, M/L, front.	S/I[2], sag., trans.	none
Univ. of Wisconsin-Milwaukee & Mayo Clinic [1]	open loop	40	20	6	M/L, front., trans.	S/I, A/P sag.	none
Cleveland Clinic [7, 26]	iterative force control	66.7 to 100	3.2	5	none	S/I, M/L, A/P front., trans., sag.	none
VA RR&D Center (RGS)	fuzzy logic control	75	2.7	9	none	S/I, M/L, A/P, front., trans., sag.	none

[1]For this system, the transverse plane rotation of the tibia can be made unconstrained by the removal of a set screw.
[2]For this system, the superior–inferior translation is indirectly prescribed via a pneumatic cylinder, which provides the vertical force.

The trajectory optimization that is employed in this study decreased the stance phase to 2.7 s: a substantial improvement compared with our previous system (10-s stance phase [10]) and many other gait simulators [1], [3]–[7] (see Table VI). Nevertheless a 2.7-s stance phase is still four times slower than the mean stance phase that is recorded *in vivo* and remains a limitation of the study.

The high stiffness inherent to parallel robots made the full BW simulation possible with the RGS [12], but the first cadaveric specimen tested failed at 100% BW, resulting in all remaining simulations being performed at 75% BW. The 75% BWs ranged from 44.3 to 51.1 kg, which is still higher than other investigators who operated at 100% BW but used specimens with the BW ranging from 35 to 50 kg (see Table VI). We recognize, however, that scaling the vGRF is still a limitation of this study and hope that younger specimens with better bone quality might allow for future simulations to occur at 100% BW.

The closed-loop fuzzy logic vGRF control greatly improved the fidelity of the vGRF as compared with the trial-and-error muscle-force-adjustment method that was previously used by our group and others [3], [6] (see Table VI). An earlier version of the RGS, which employed the trial-and-error vGRF control, had a vGRF RMS tracking error of 30.0% BW [10]. The fuzzy logic vGRF controller used in this study was able to reduce this to 5.6% BW.

There are several small but notable limitations of the vGRF tracking performance. The *in vitro* vGRF was typically below the target *in vivo* vGRF shortly after heel strike (see Fig. 7). This is likely the result of the reduced simulation velocity. Increasing the simulation velocity would increase the rotational plantar flexion acceleration of the foot just after heel strike and result in a larger vGRF at this time. A greater velocity also might better model the heel-strike impulse typical of the *in vivo* vGRF.

The second notable performance limitation of the fuzzy logic vGRF controller is the consistent undershoot of the first peak of the vGRF (see Fig. 7). The undershoot most likely results from the definition of the membership functions for the fuzzy subsets LN, SN, *Z*, SP, and LP for the input variable $\mathrm{vGRF}_{\mathrm{error}}$. These membership functions were designed purposefully to reduce high-frequency Δx oscillations by creating a dead band in the output variable Δx for very small values of $\mathrm{vGRF}_{\mathrm{error}}$. The consistent undershoot was likely created by this dead band and the fact that the vGRF was typically below the target vGRF when the fuzzy logic vGRF was enabled. Decreasing the dead band and increasing the fuzzy logic vGRF responsiveness to small values of $\mathrm{vGRF}_{\mathrm{error}}$ would likely reduce the undershoot.

The third limitation of the vGRF tracking is the minimum between peaks being persistently below the target at approximately 43% of the stance phase (see Fig. 7). This undershoot, which is present when the Ach tendon fuzzy logic controller becomes active, results in the Ach tendon force quickly increasing to compensate (see Fig. 11). This behavior, as well as the *in vitro* second peak vGRF, being on average 1.7% below the target, might be resolved through further tuning of the fuzzy sets.

V. CONCLUSION

In this paper, the RGS, i.e., a novel dynamic cadaveric gait simulator, has been developed and validated. A fuzzy logic vGRF controller has been designed, which iteratively altered the tibial kinematics and the TA and Ach tendon forces in real time in order to control the vGRF with greater fidelity than the current state of the art. A parallel robot has been used to accurately and repeatable prescribe TIB with respect to GND

kinematics. The RGS is a useful tool for biomechanics investigations of normal and pathologic feet.

REFERENCES

[1] K. Kim, H. B. Kitaoka, Z. Luo, S. Ozeki, L. J. Berglund, K. R. Kaufman, and K. An, "In vitro simulation of the stance phase in human gait," *J. Musculoskeletal Res*., vol. 5, pp. 113–122, Jun. 2001.

[2] C. J. Nester, A. M. Liu, E. Ward, D. Howard, J. Cocheba, T. Derrick, and P. Patterson, "In vitro study of foot kinematics using a dynamic walking cadaver model," *J. Biomech*., vol. 40, pp. 1927–1937, 2007.

[3] N. Okita, S. Meyers, J. Challis, and N. Sharkey, "An objective evaluation of a segmented foot model," *Gait Posture*, vol. 30, pp. 27–34, Jul. 2009.

[4] C. Hurschler, J. Emmerich, and N. Wulker, "In vitro simulation of stance phase gait—Part I: Model verification," *Foot Ankle Int*., vol. 24, pp. 614–622, Aug. 2003.

[5] N. Wülker, C. Hurschler, and J. Emmerich, "In vitro simulation of stance phase gait—Part II: Simulated anterior tibial tendon dysfunction and potential compensation," *Foot Ankle Int*., vol. 24, pp. 623–629, Aug. 2003.

[6] Y. M. Kirane, J. D. Michelson, and N. A. Sharkey, "Evidence of isometric function of the flexor hallucis longus muscle in normal gait," *J. Biomech*., vol. 41, pp. 1919–1928, 2008.

[7] D. Lee and B. Davis, "Assessment of the effects of diabetes on midfoot joint pressures using a robotic gait simulator," *Foot Ankle Int*., vol. 30, pp. 767–772, Aug. 2009.

[8] S. W. Donahue, N. A. Sharkey, K. A. Modanlou, L. N. Sequeira, and R. B. Martin, "Bone strain and microcracks at stress fracture sites in human metatarsals," *Bone*, vol. 27, pp. 827–833, Dec. 2000.

[9] E. D. Ward, K. M. Smith, J. R. Cocheba, P. E. Patterson, and R. D. Phillips, "In vivo forces in the plantar fascia during the stance phase of gait: Sequential release of the plantar fascia," *J. Am. Podiatric Med. Assoc*., vol. 93, pp. 429–442, Feb. 2009.

[10] A. F. Bayomy, P. M. Aubin, B. J. Sangeorzan, and W. R. Ledoux, "Arthrodesis of the first metatarsophalangeal joint: A robotic cadaveric study of dorsiflexion angle," *J. Bone Joint Surgery Amer*., vol. 92, no. 8, pp. 1754–1764, Jul. 21, 2010.

[11] J. D. Michelson, A. J. Hamel, F. L. Buczek, and N. A. Sharkey, "Kinematic behavior of the ankle following malleolar fracture repair in a high-fidelity cadaver model," *J. Bone Joint Surgery*., vol. 84-A, pp. 2029–2038, Nov. 2002.

[12] P. Aubin, M. Cowley, and W. Ledoux, "Gait simulation via a 6-DOF parallel robot with iterative learning control," *IEEE Trans. Biomed. Eng*., vol. 55, no. 3, pp. 1237–1240, Mar. 2008.

[13] A. Hoskins, "Development and characterization of a robotic dynamic activity simulator," M.S. thesis, Dept. Mech. Eng., Penn. State Univ., Philadelphia, 2006.

[14] S. S. Farinwata, D. P. Filev, and R. Langari, *Fuzzy Control: Synthesis and Analysis*. Hoboken, NJ: Wiley, 2000.

[15] T. Ross, *Fuzzy Logic with Engineering Applications*. Chichester, U.K: Wiley, 2005.

[16] L. Tian, "An intelligent control method based on fuzzy logic for a robotic testing system for the human spine," *J. Biomech. Eng*., vol. 127, pp. 807–812, Oct. 2005.

[17] T. Wickiewicz, R. Roy, P. Powell, and V. Edgerton, "Muscle architecture of the human lower limb," *Clin. Orthopaedics Related Res*., vol. 179, pp. 275–283, 1983.

[18] T. Fukunaga, R. Roy, F. Shellock, J. Hodgson, and V. Edgerton, "Specific tension of human plantar flexors and dorsiflexors," *J. Appl. Physiol*., vol. 80, pp. 158–165, Jan. 1996.

[19] J. Perry, *Gait Analysis*. Thorofare, NJ: Slack, 1992.

[20] S. Zhou, D. Lawson, W. Morrison, and I. Fairweather, "Electromechanical delay in isometric muscle contractions evoked by voluntary, reflex, and electrical-stimulation," *Eur. J. Appl. Physiol. Occupat. Physiol*., vol. 70, pp. 138–145, Feb. 1995.

[21] M. Ishikawa, P. Komi, M. Grey, V. Lepola, and G. Bruggemann, "Muscle-tendon interaction and elastic energy usage in human walking," *J. Appl. Physiol*., vol. 99, pp. 603–608, Aug. 2005.

[22] E. Mamdani, "Application of fuzzy logic to approximate reasoning using linguistic synthesis," *IEEE Trans. Comput*., vol. C-26, no. 12, pp. 1182–1191, Dec. 1977.

[23] Z. Kovacic, *Fuzzy Controller Design: Theory and Applications*. Boca Raton, FL: CRC/Taylor & Francis, 2006.

[24] A. Erdemir, M. Viveiros, J. Ulbrecht, and P. Cavanagh, "An inverse finite-element model of heel-pad indentation," *J. Biomech*, vol. 39, pp. 1279–1286, 2006.

[25] R Development Core Team, *A Language and Environment for Statistical Computing*. Vienna, Austria: R Foundation for Statistical Computing, 2009.

[26] L. D. Noble, Jr., R. W. Colbrunn, D. G. Lee, A. J. van den Bogert, and B. L. Davis, "Design and validation of a general purpose robotic testing system for musculoskeletal applications," *J. Biomech. Eng*., vol. 132, no. 2, pp. 025001-1–025001-12, Feb. 2010.

Patrick M. Aubin (M'03) received the B.S., M.S., and Ph.D. degrees from the University of Washington, Seattle, all in electrical engineering, in 2004, 2006, and 2010, respectively.

He was a Research Assistant with the Department of Veterans Affairs, VA Puget Sound Health Care System, Seattle, from 2005 to 2010. Currently, he is a Visiting Scholar with the Department of Biomechanics, Vilnius Gediminas Technical University, Vilnius, Lithuania. His research interest includes biomedical robotics and controls.

Dr. Aubin received the 2010 Whitaker International Scholar and the U.S. Student Fulbright awards.

Eric Whittaker received the B.S. degree in biomedical engineering from the Georgia Institute of Technology, Atlanta, in 2005 and the M.S. degree in biomechanics from the University of California, Davis, in 2009.

He has been a Research Biomedical Engineer with the Department of Veterans Affairs, VA Puget Sound Health Care System, Seattle, WA, since 2009.

William R. Ledoux received the B.S. degree in biomedical engineering from Rensselaer Polytechnic Institute, Troy, NY, in 1992 and the M.S. and Ph.D. degrees in bioengineering from the University of Pennsylvania, Philadelphia, in 1993 and 1999, respectively.

He has been a Research Biomedical Engineer with the Department of Veterans Affairs, VA Puget Sound Health Care System, Seattle, WA, since 1999. He is currently an Affiliate Associate Professor with the Department of Mechanical Engineering and with the Department of Orthopaedics and Sports Medicine, University of Washington. His research interests include foot-type biomechanics, soft tissue mechanical testing, and the relationship between foot structure and diabetic foot ulceration.